Authorized Reprint from
Special Technical Publication 803, Vol. I

1984

Ming Yuan He[1] *and John W. Hutchinson*[2]

Penny-Shaped Crack in a Round Bar of Power-Law Hardening Material

REFERENCE: He, M. Y. and Hutchinson, J. W., **"Penny-Shaped Crack in a Round Bar of Power-Law Hardening Material,"** *Elastic-Plastic Fracture: Second Symposium, Volume I—Inelastic Crack Analysis, ASTM STP 803*, C. F. Shih and J. P. Gudas, Eds., American Society for Testing and Materials, 1983, pp. I-291–I-305.

ABSTRACT: A study is made of the deformation of a round bar of pure power-law hardening material under tension containing a central penny-shaped crack. Several important issues related to fracture mechanics are examined, including the near-tip stress and strain field and its relation to the analogous problem in plane strain.

KEY WORDS: nonlinear fracture mechanics, penny-shaped crack, J-integral, fully plastic crack problems, elastic-plastic fracture

This paper continues a study initiated in a previous paper [*1*][3] in which the problem of a penny-shaped crack in an infinite body subject to general remote axisymmetric stressing conditions was studied. Now the objective is the finite problem of a round bar containing a centered penny-shaped crack.

The material is an incompressible, isotropic solid. A pure power hardening relation between stress and strain is assumed so that in simple tension

$$\epsilon/\epsilon_0 = \alpha(\sigma/\sigma_0)^n \tag{1}$$

where ϵ_0 and σ_0 are a reference strain and stress and α is an extra constant introduced for convenience of application. For J_2 deformation theory, Eq 1 generalizes to

$$\frac{\epsilon_{ij}}{\epsilon_0} = \frac{3}{2}\,\alpha\left[\frac{\sigma_e}{\sigma_0}\right]^{n-1}\frac{S_{ij}}{\sigma_0} \tag{2}$$

[1]Researcher, Institute of Mechanics, Chinese Academy of Sciences, Beijing, China.
[2]Professor of applied mechanics, Division of Applied Sciences, Harvard University, Cambridge, Mass. 02138.
[3]The italic numbers in brackets refer to the list of references appended to this paper.

where S_{ij} is the stress deviator and σ_e is the effective stress defined by

$$\sigma_e = \left(\frac{3}{2} S_{ij} S_{ij}\right)^{1/2} \tag{3}$$

It is also convenient to define an effective strain

$$\epsilon_e = \left(\frac{2}{3} \epsilon_{ij} \epsilon_{ij}\right)^{1/2} \tag{4}$$

which coincides with the tensile strain in uniaxial tension so that σ_e and ϵ_e satisfy Eq 1. A catalog of fully plastic solutions for this class of materials is now available [*2*].

The incompressible finite-element program (INFEM) developed by Needleman and Shih [*3*] will be used. In this program the incompressibility constraints are imposed directly on the nodal degrees of freedom. We recapitulate briefly the method which has been explained in detail in Ref *3*.

The basic finite element employed is a quadrilateral composed of four constant-strain triangles arranged so that the diagonals and edges of the quadrilateral form the sides of the triangles as depicted in Fig. 1. For each triangle in the quadrilateral there is one constraint equation arising from the incompressibility condition. For each quadrilateral there are four such equations, but only three of these are independent. Two of these three constraint equations can be used to express the nodal displacements of the central node of the quadrilateral in terms of the nodal displacements of the corners. Therefore there is only one independent constraint to be satisfied in each quadrilateral. The quadrilaterals are arranged in strips ranging from one boundary of the grid to another, as shown in Fig. 2. Two such strips are considered as one substructure, and the centerline of nodes is employed to satisfy the remaining constraints.

Problem and Method

Axisymmetric fully plastic analyses were carried out for a round bar of radius b under uniform tension containing a central penny-shaped crack of radius a, shown in Fig. 3, for $a/b = 0.25, 0.5, 0.75$ and $n = 1, 3, 5, 10$. As a comparison, analyses were also carried out for a plane-strain center-cracked panel (CCP) under remote uniform tension for $a/b = 0.25$, $n = 1, 3, 5, 10$

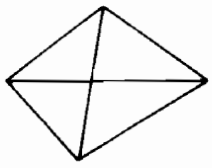

FIG. 1—*Quadrilateral element.*

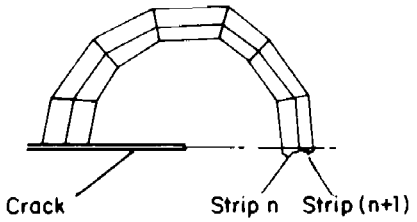

FIG. 2—*Strip arrangement of elements.*

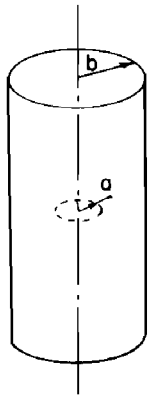

FIG. 3—*Geometry of round bar with penny-shaped crack.*

and $a/b = 0.75$, $n = 1, 3, 5$. Because of the symmetry with respect to the crack, only the upper half of the specimen was modeled. A typical finite-element mesh for the case $a/b = 0.25$ is shown in Fig. 4; the mesh has 12 quadrilateral elements in circumferential direction about the crack tip and 27 elements in the radial direction from the tip to the external boundaries. The meshes used for the other ratios a/b were similar to the one shown here. The meshes have a small hole at the crack tip with radius equal to 1 to 2 percent of the crack length or the remaining ligament, whichever is the smaller dimension. According to Ref *4*, this hole has virtually no effect on the J-integral and mouth opening displacement for $n = 1 \sim 20$ for plane-strain fully plastic analysis.

The INFEM program employs linear or modified Newton-Raphson iteration to obtain the desired solution. The parameter tracking technique was used by which the solution corresponding to $n = 1$ was taken as the initial guess to obtain the solution for $n = 3$ and which in turn is used as the initial guess to obtain the solution for $n = 5$ and so on. In our calculation, for $a/b = 0.25$ and 0.5, Newton's iterations were used. It typically took three or four iterations to reach the desired accuracy. For $a/b = 0.75$, several linear iterations were used at the start and then Newton's procedure was used to obtain convergence.

For convenience, uniform displacement boundary conditions were imposed

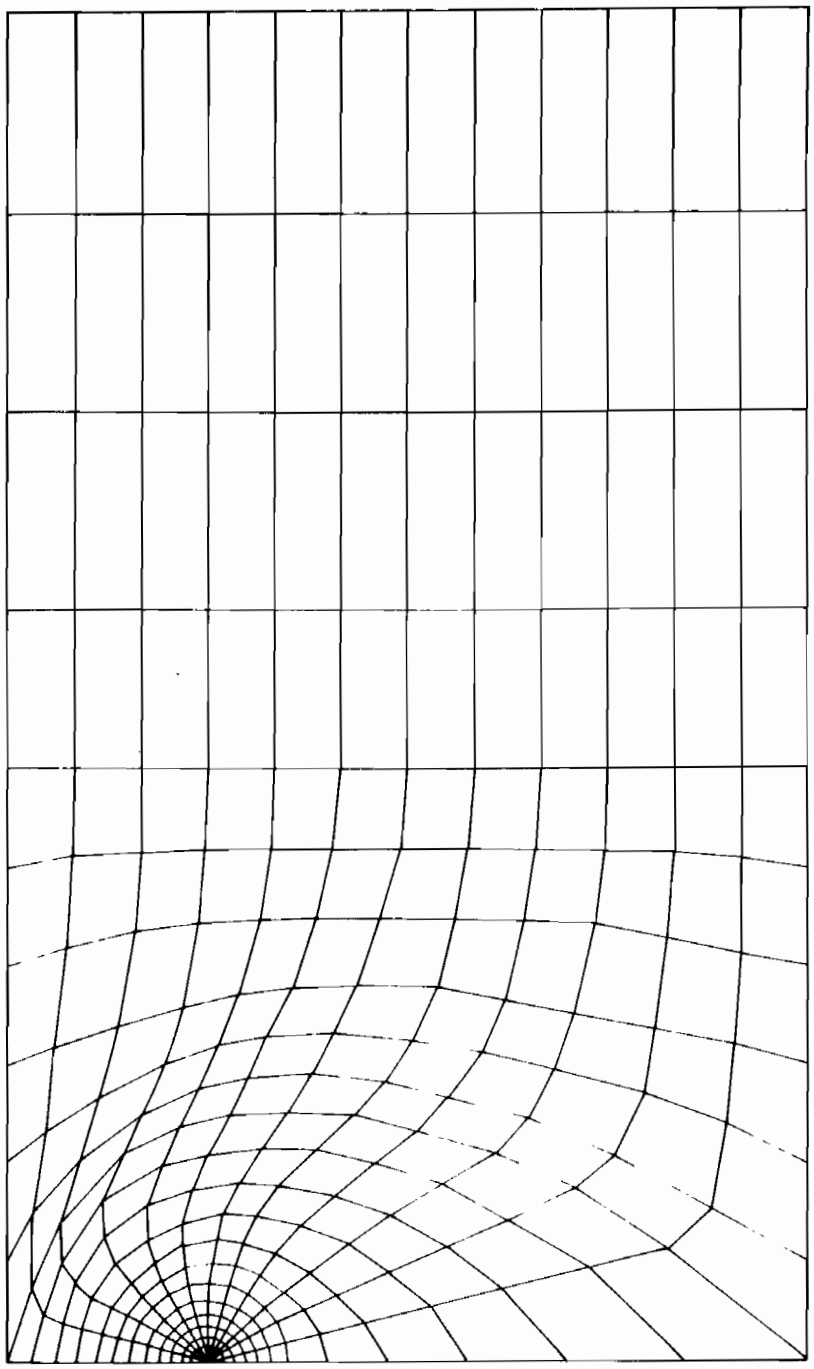

FIG. 4—*Finite-element mesh for* a/b = 1/4.

on the ends. ($L/b = 1.7$ for $a/b = 0.25$ and $L/b = 2.3$ for $a/b = 0.75$, where $2L$ is the length of the bar.) The results show that the stresses on the end boundary are very close to uniform tension.

For the axisymmetric problem the M-integral was evaluated. For the power-law material, the M-integral is given by [5]

$$M = \int_S \left[W x_i n_i - \sigma_{ij} n_j u_{i,k} x_k - \frac{(2n-1)}{(n+1)} \sigma_{ij} n_j u_i \right] ds \tag{5}$$

where

$$w(\epsilon) = \int_0^{\epsilon} \sigma_{ij} d\epsilon_{ij} = \frac{n}{n+1} \alpha \sigma_0 \epsilon_0 \left[\frac{\epsilon_e}{\alpha \epsilon_0} \right]^{(n+1)/n} \tag{6}$$

and S is any closed surface which encloses the crack and n is the unit outward normal to S at each point. If J is defined as the energy release rate per unit length of crack edge for a penny-shaped crack in a round bar as in the plane case, that is

$$J = -\frac{1}{2\pi a} \frac{dPE}{da} \tag{7}$$

where PE is the potential energy of the cracked body, then it follows that

$$J = \frac{M}{2\pi a^2} \tag{8}$$

As discussed in Ref *1*, J also plays the role of the amplitude of the plane-strain crack-tip singularity fields which dominate as the crack is approached. As a check on the numerical accuracy, the M-integral was evaluated along a number of torus-like surfaces ringing the edge of the penny-shaped crack. In all cases the computed values of M were found to be within about 1 percent of the mean value (over all the surfaces).

Results and Discussion

Results for J-Integral and Crack-Opening Displacement

The normalizations of J and δ_0 are given by

$$h_1 = \frac{J}{\sigma_e^{\infty} \epsilon_e^{\infty} a} [1 - (a/b)^2]^n$$

$$h_2 = \frac{\delta_0}{a \epsilon_0^{\infty}} [1 - (a/b)^2]^n \tag{9}$$

where σ_e^∞ and ϵ_e^∞ are the remote effective stress and effective strain which satisfy the power-law relation, Eq 1, and δ_0 is the opening of the crack at its center. Numerical results for h_1 and h_2 for $a/b = 0.25, 0.5, 0.75$ and $n = 1, 3, 5, 10$ are given in Table 1 and Figs. 5 and 6. The results for h_1 and h_2 for $a/b = 0$ from Ref *1* are also included for comparison purposes.

TABLE 1—h_1 *and* h_2 *for penny-shaped crack in a round bar.*

$$h_1 = \frac{J(1-(a/b)^2)^n}{\sigma_e^\infty \epsilon_e^\infty a}$$

a/b	$n = 1$	$n = 3$	$n = 5$	$n = 10$
0	0.9549	1.331	1.484	1.639
0.25	0.9369	1.267	1.335	1.264
0.5	0.8350	0.9163	0.8379	0.5520
0.75	0.8010	0.5959	0.3926	0.1334

$$h_2 = \frac{\delta_0(1-(a/b)^2)^n}{\epsilon_e^\infty a}$$

a/b	$n = 1$	$n = 3$	$n = 5$	$n = 10$
0	1.909	2.375	2.525	2.637
0.25	1.858	2.131	2.107	1.819
0.5	1.626	1.451	1.183	0.6631
1.0	0.7957	0.4369	0.2640	0.08439

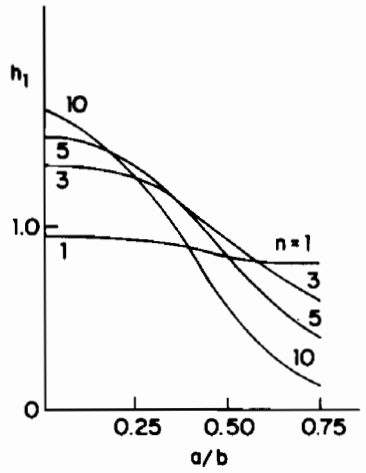

FIG. 5—$h_1(a/b, n)$ *defined in Eq 9.*

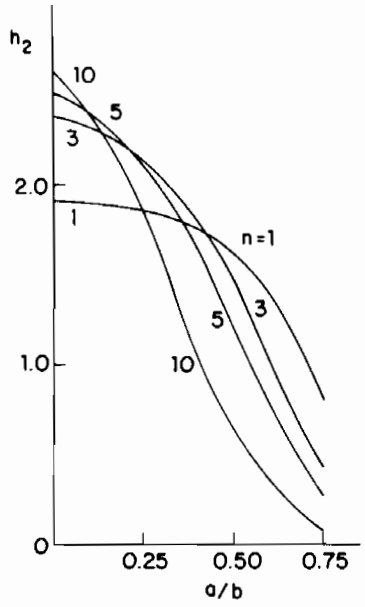

FIG. 6—$h_2(a/b, n)$ *defined in Eq 9.*

The present results for the linear elastic case corresponding to $n = 1$ were compared with the results of Benthem [*6*]. It was found that for all a/b, the averages of the J-integral over all the valid contours enclosing the crack tip were within 3 percent of the values given in Ref *6*.

Stress Field Near the Crack Tip

According to Hutchinson-Rice-Rosengren (HRR) theory [*7,8*] for a plane-strain crack the stress field of the dominant singularity at the crack tip has the form

$$\sigma_{ij} = \sigma_0 \left[\frac{J}{\alpha \sigma_0 \epsilon_0 I_n r} \right]^{1/(n+1)} \tilde{\sigma}_{ij}(\theta, n) \tag{10}$$

where r is the distance from the crack tip and θ is the angle measured from directly ahead of the crack. The plane-strain singular fields, Eq 10, also hold at the edge of a penny-shaped crack, where r and θ are then local coordinates in a plane perpendicular to the edge of the crack. At issue is the size of the crack-tip region over which the singular field, Eq 10, dominates. We compared the calculated stress distributions from the finite-element method with the HRR field. The normal stress ahead of the crack σ_{yy} is normalized in the following way

$$\frac{\sigma_{yy}/\sigma_e^{\infty}}{\left(\dfrac{J}{\sigma_e^{\infty}\epsilon_e^{\infty}a}\right)^{1/(n+1)}} = \frac{\sigma_{yy}/\sigma_0}{\left(\dfrac{J}{\alpha\sigma_0\epsilon_0 a}\right)^{1/(n+1)}} \tag{11}$$

which is necessarily independent of J (and of load). According to HRR theory, from Eq 10

$$\frac{\sigma_{yy}/\sigma_0}{\left(\dfrac{J}{\alpha\sigma_0\epsilon_0 a}\right)^{1/(n+1)}} = \left(\frac{a}{rI_n}\right)^{1/(n+1)} \tilde{\sigma}_{yy}(0, n) \tag{12}$$

where I_n is an integration constant. I_n and $\tilde{\sigma}_{yy}$ can be found in Ref *7*.

The plots of this ratio are given in Fig. 7 for $n = 1$, 3, and 10 and $a/b = 0.25$ and 0.75. The corresponding curves for the plane-strain centered crack are also included. It is seen that for the penny-shaped crack the normalized normal stress ahead of the crack falls well below that for the HRR singular field where $r/a > 0.02$ when $n \geq 3$. For $r/a < 0.02$ our finite-element resolution of

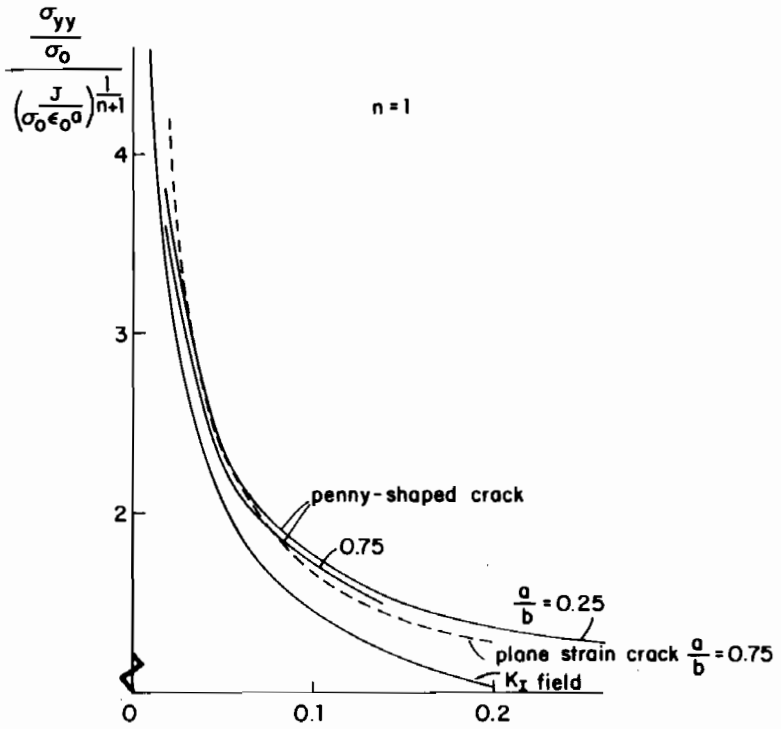

FIG. 7*a*—*Normalized stress ahead of crack edge for* n = *1.*

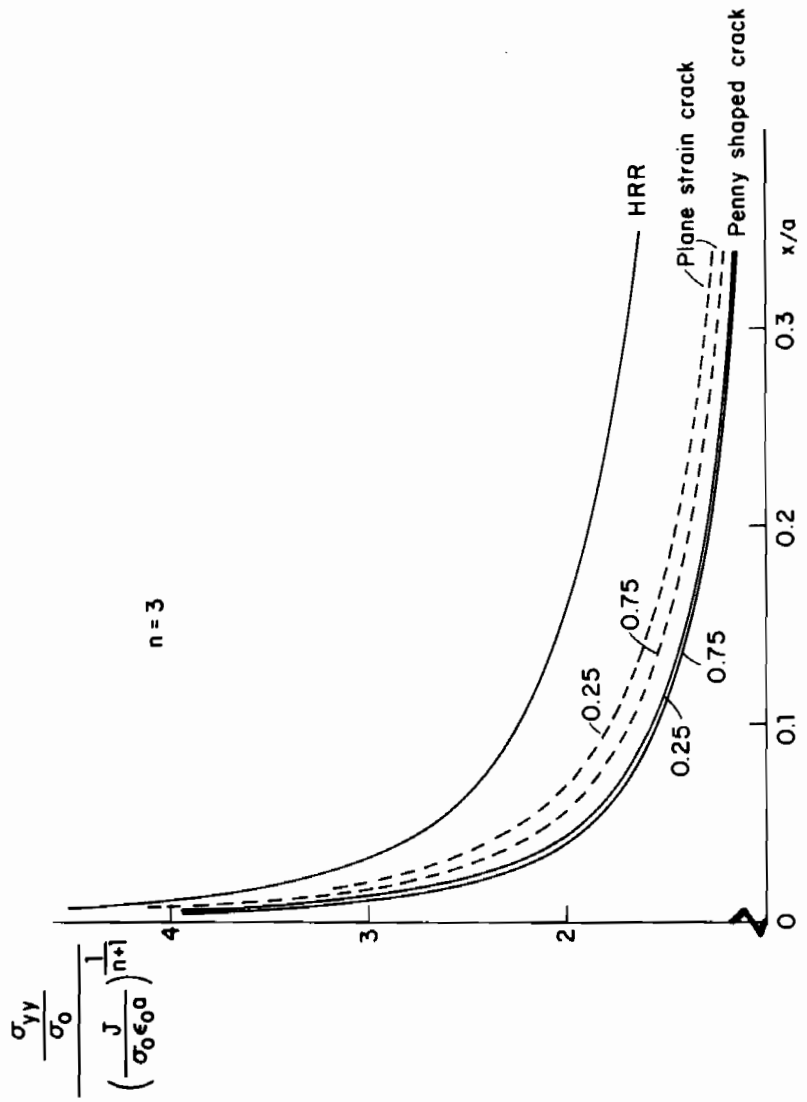

FIG. 7b—*Normalized stress ahead of crack edge for* n = 3.

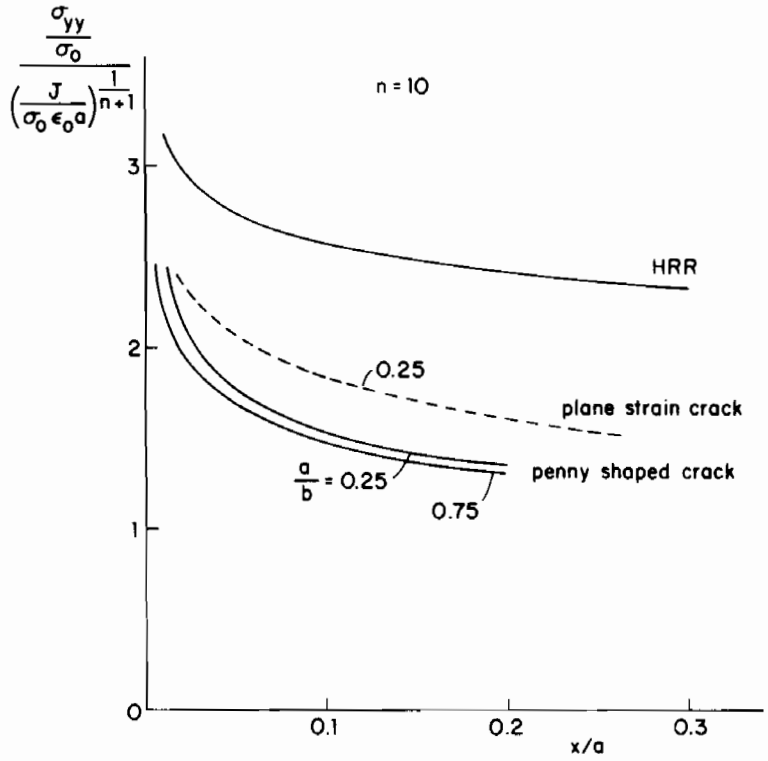

FIG. 7c—*Normalized stress ahead of crack edge for* n = *10.*

the stress field is not sufficient to make a more accurate comparison. What is clear, however, is that the size of the region in which the stresses are well approximated by the singular field is less than about $0.02a$. It should be noted that for a given n these curves depend only slightly on a/b and the differences between the results of the penny-shaped crack and the plane-strain crack are relatively small.

Displacement and Near-Tip Strain of the Bar

A significant difference between the axisymmetric problem and the plane-strain problem is brought out by the plots of Fig. 8, which show the displacement of the boundaries for the case $a/b = 0.25$ and $n = 10$. Included in the figure for the plane-strain specimen is the rigid-perfectly plastic slipline mode of deformation. It is seen that the solution for $n = 10$ reflects the limiting discontinuous behavior of the perfectly plastic solution. By contrast, no slip discontinuities are possible in the perfectly plastic axisymmetric problem and, in fact, it can be seen that the presence of the crack does not significantly per-

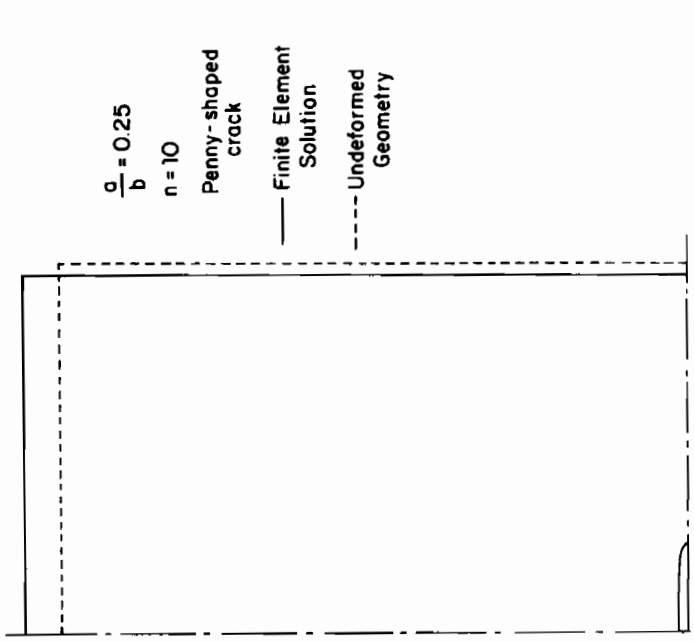

FIG. 8b—*Displacement of boundary for round bar with penny-shaped crack.*

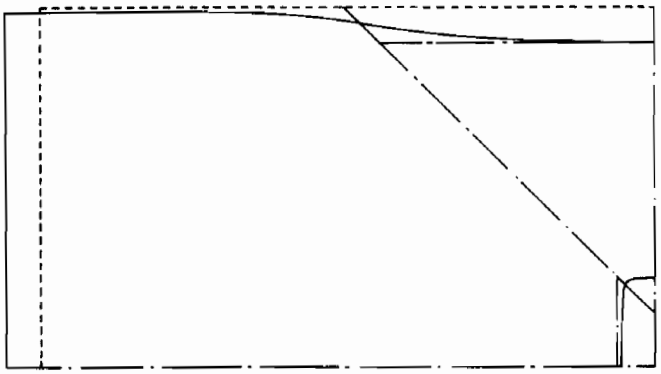

FIG. 8a—*Displacement of the boundary for the plane-strain problem and comparison with the slipline solution for the rigid-perfectly plastic limit.*

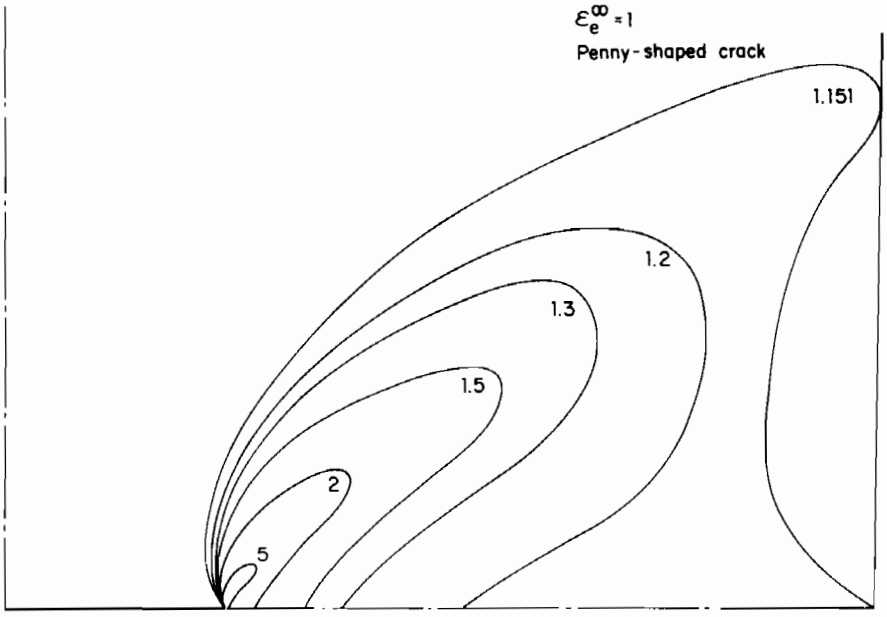

FIG. 9—*Contours of constant effective strain* ϵ_e *for penny-shaped crack in round bar with* n = *10,* a/b = *¼, and* $\epsilon_e^\infty = 1$.

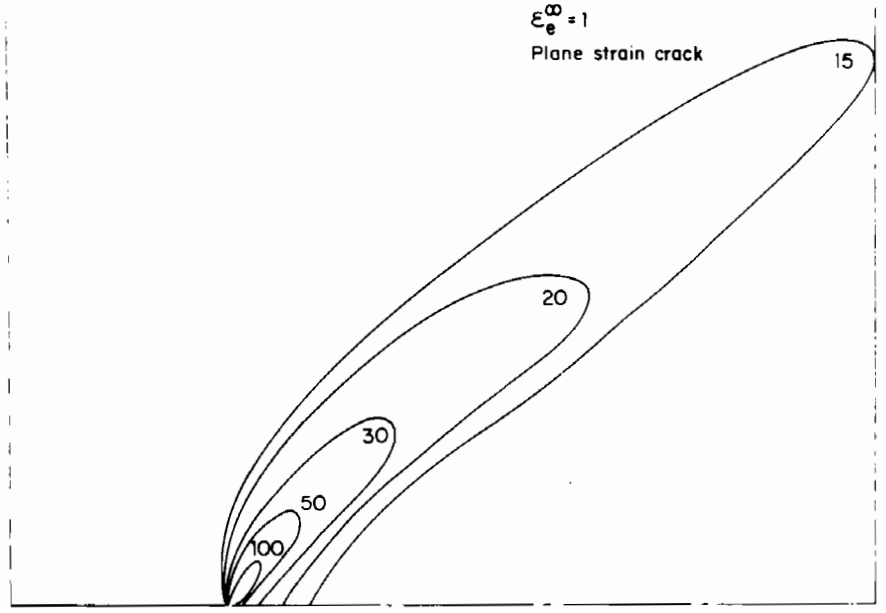

FIG. 10—*Contours of constant effective strain* ϵ_e *for plane-strain crack-problem with* n = *10,* a/b = *¼, and* $\epsilon_e^\infty = 1$.

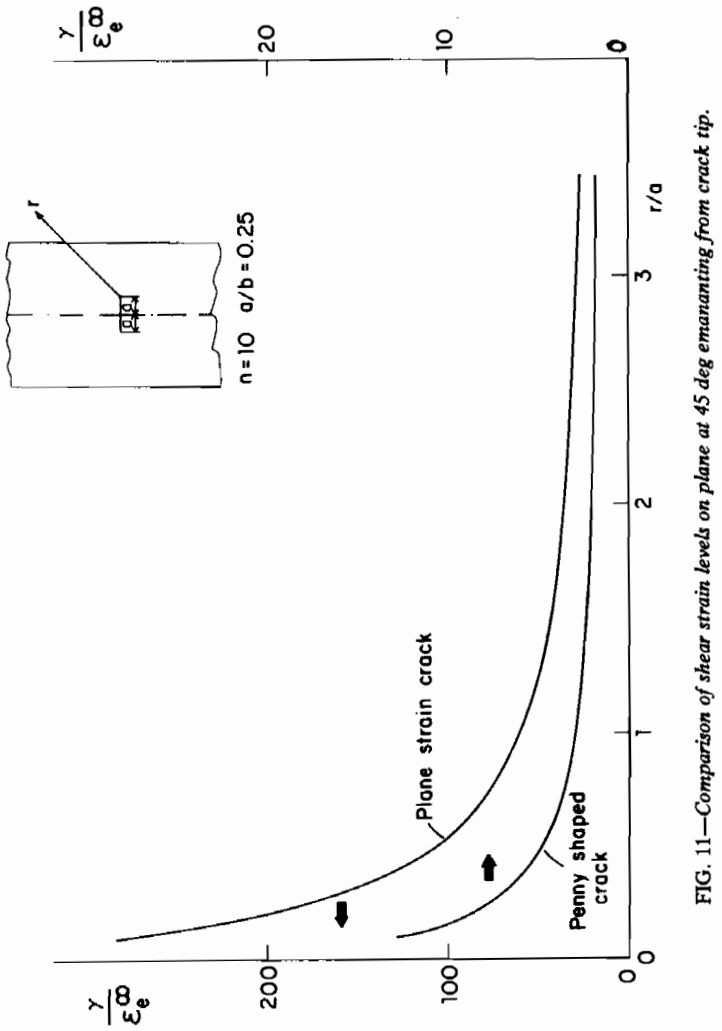

FIG. 11—*Comparison of shear strain levels on plane at 45 deg emananting from crack tip.*

turb the boundary of this specimen. Contours on which the effective strain is a constant are shown in Fig. 9 for the penny-shaped crack and in Fig. 10 for the plane-strain crack, both for $n = 10$, $a/b = 0.25$, and loaded such that $\epsilon_e^\infty = 1$. Obviously, there are significant differences between these two cases. For the plane-strain case the strain concentrates in rather narrow bands emanating from the tips. On the other hand, for the penny-shaped crack, the strain field is much more diffuse. A comparison of Fig. 10 with Fig. 9 reveals the substantially larger strain concentration in the plane-strain problem at a given distance from the curve tip.

The shear strains ($\gamma \equiv 2\epsilon_{r\theta}$) on the 45-deg line emanating from the tip are shown in Fig. 11. It is again seen that for the plane-strain crack the shear strain is 15 to 20 times higher than the shear strain for the penny-shaped crack.

Finally, to aid in obtaining the limit load for the rigid-perfectly plastic penny-shaped cracked round bar, we define as σ_L^∞ the remote stress at which ϵ_e first attains the value ϵ_0 at the outer cylindrical boundary. Computed values of $\sigma_L^\infty/\{\sigma_0[1 - (a/b)^2]\}$ are shown as solid lines in Fig. 12 for $n = 1$, 3, 5, and 10. The dashed curve for $n = \infty$ is the estimate of the limit load and this was obtained by cross-plotting against $1/n$ and extrapolating to the limit $n \to \infty$ for given values of a/b.

Acknowledgment

We are indebted to A. Needleman and C. F. Shih for supplying us with a copy of their finite-element program INFEM and for helpful discussions. This

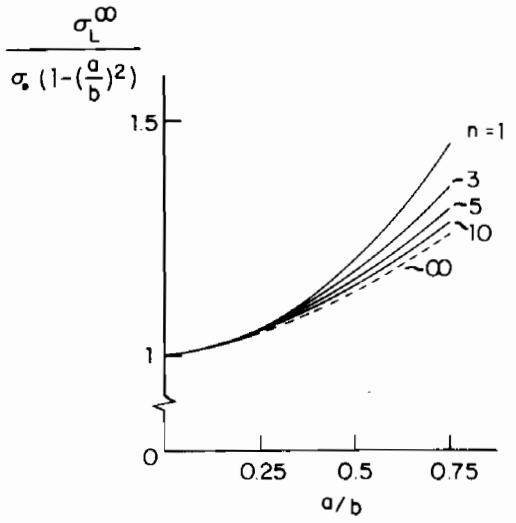

FIG. 12—*Remote stress* σ_L^∞ *at which* ϵ_e/ϵ_0 *first attains unity at the external surface of a round bar, and extrapolation to limit load corresponding to* $n = \infty$.

work was supported in part by the National Science Foundation under Grants DMR-80-20247 and CME-78-10756, and by the Division of Applied Sciences, Harvard University.

References

[1] He, M. Y. and Hutchinson, J. W., *Journal of Applied Mechanics*, Vol. 48, 1981, pp. 830–840.
[2] Kumar, V., German, M. D., and Shih, C. F., "An Engineering Approach for Elastic-Plastic Fracture Analysis," NP-1931, Research Project 1237-1. Prepared for Electric Power Research Institute, Palo Alto, Calif., 1981.
[3] Needleman, A. and Shih, C. F., *Computer Methods in Applied Mechanics and Engineering*, Vol. 15, 1978, pp. 223–240.
[4] Shih, C. F. and Kumar, V., "Estimation Technique for the Prediction of Elastic-Plastic Fracture of Structural Components of Nuclear Systems." First Semiannual Report, General Electric Co., Schenectady, N.Y., 1 June 1979.
[5] Budiansky, B. and Rice, J. R., *Journal of Applied Mechanics*, Vol. 40, 1973, pp. 201–203.
[6] Tada, H., Paris, P. C., and Irwin, G. R., *The Stress Analysis of Cracks Handbook*, Del Research Corp., Hellertown, Pa., 1973, p. 28.1.
[7] Hutchinson, J. W., *Journal of the Mechanics and Physics of Solids*, Vol. 16, 1968, pp. 13–31.
[8] Rice, J. R. and Rosengren, G. K., *Journal of the Mechanics and Physics of Solids*, Vol. 16, 1968, pp. 1–12.